



Contents lists available at ScienceDirect

Engineering Science and Technology, an International Journal

journal homepage: www.elsevier.com/locate/jestch



Study on thermal performance and simulation method of oil medium steel-BMC mechanical joints



Jiaxing Shen ^{a,b,*}, Zihao Pan ^b, Yu Chen ^b, Ping Xu ^b, Yinghua Yu ^b

^a Research Institute of Technology and Equipment for the Exploitation and Utilization of Mineral Resources, Liaoning Technical University, Fuxin 123000, China

^b School of Mechanical Engineering, Liaoning Technical University, Fuxin 123000, China

ARTICLE INFO

Article history:

Received 24 March 2023

Revised 1 June 2023

Accepted 29 June 2023

Available online 11 July 2023

Keywords:

Oil-medium

Steel-BMC mechanical joints

Actual contact proportion

Thermal performance

ABSTRACT

In order to study the thermal performance and simulation analysis method of oil medium steel-BMC mechanical joints. Discrete analytical methods of the actual solid contact proportion and actual lubricating oil contact proportion of the oil medium steel-BMC mechanical joints were established respectively. A theoretical model of the thermal behaviour parameters and equivalent thickness of the oil medium steel-BMC mechanical joints was developed and the influence of preload and roughness on its thermal behaviour parameters was investigated. A virtual material-simulation analysis method for oil medium steel-BMC mechanical joints considering contact weights has been developed. The temperature variation of oil medium steel-BMC mechanical joint specimens was investigated using virtual material-simulation analysis methods and experimental methods. It was found that the maximum relative error between the two methods is -2.1%, verifying the validity of the analytical method for the actual contact proportion of oil medium steel-BMC mechanical joints and the theoretical model for the thermal behaviour parameters of oil medium steel-BMC mechanical joints. Finally, the thermal performance and thermal mechanical coupling performance of the BMC bed foundation were investigated through simulation analysis, proving that the oil medium steel-BMC mechanical joints have a significant impact on the overall performance of the machine tool.

© 2023 Karabuk University. Publishing services by Elsevier B.V. This is an open access article under the CC BY-NC-ND license (<http://creativecommons.org/licenses/by-nc-nd/4.0/>).

1. Introduction

Mineral composite (MC) materials have the characteristics of high damping, high thermal stability, high ratio of stiffness to mass, etc. Using mineral composites as the basic components of a machine tool is one of the effective ways to improve its machining accuracy and performance [1–6]. The mineral composite material studied in this paper is a new type of mineral composite material, which is mainly composed of basalt aggregate, basalt fiber, fly ash, epoxy resin, etc., abbreviated as BMC. The BMC has a high damping ratio, specific heat capacity, stiffness to mass ratio and strength to mass ratio. In addition, it has the advantages of simple manufacturing process, short curing period and rich raw materials, etc [7]. Therefore, the use of BMC materials to manufacture machine tools can significantly improve the static, dynamic and thermal properties of machine tools. BMC material can be machined into the basic components of machine tools, such as

machine beds and columns. The steel parts of the machine and the BMC base parts combine to form a steel BMC mechanical joint. Because the machined surface is rough and its surface has many micro-convex peaks, the actual contact area of the mechanical joints is a fraction of the nominal contact area. There are numerous tiny pores within the mechanical joints [8–10]. The guideway of the machine tool is usually lubricated with rich oil when it is working. The excess lubricant oil fills the gap in the mechanical joint and constitutes the oil medium steel-BMC mechanical joints. The thermal and dynamic properties of oil medium steel-BMC mechanical joints differ markedly from those of conventional steel and BMC materials. Therefore, the oil medium steel-BMC mechanical joint has a fundamental influence on the thermal performance, dynamic performance and thermomechanical coupling properties of the machine tool [11].

Currently, researches on mechanical joints are mostly focused on the performance of metal mechanical joints for conventional machine tools. For example, Shoukry [12] studied the contact stiffness of mechanical joints and developed a corresponding mathematical model. He also found that mechanical joints have a constant tangential-normal contact stiffness ratio. Archenti [13] studied the proportion of the mechanical joints errors to the total

* Corresponding author at: Research Institute of Technology and Equipment for the Exploitation and Utilization of Mineral Resources, Liaoning Technical University, Fuxin 123000, China.

E-mail addresses: 329833309@qq.com, shenjiaxing@lntu.edu.cn (J. Shen).

error of the machine. He found that the accuracy of the machine tools is largely affected by the mechanical joints. Zhao [14] deduced the elastic modulus and shear modulus of the mechanical joints based on the fractal contact theory. Chen [10] investigated the effect of friction on the contact stiffness of mechanical joints and developed a model for the contact stiffness considering the effect of friction. It can be seen that very little research has been carried out on the performance of oil medium steel-BMC mechanical joints.

This paper investigates the thermal characteristics of oil medium steel-BMC mechanical joints. A new discrete analytical method for the actual contact proportion of oil medium steel-BMC mechanical joints considering contact weight was developed. The variation pattern of the actual contact proportion with preload and roughness is analysed. A model of the thermal parameters of the oil medium steel-BMC mechanical joints was developed. The virtual material-simulation analysis method of oil medium steel-BMC mechanical joints was established theoretically, and the accuracy of the theoretical model and simulation analysis method was verified through experiments and simulations. Taking certain type of BMC bed foundation as an example, the influence of oil medium steel-BMC mechanical joints on thermal performance and thermal mechanical coupling characteristics of BMC bed foundation was studied. The important influence of thermal properties and thermal mechanical coupling characteristics of oil medium steel-BMC mechanical joints is proved.

2. Analysis of actual contact proportion

2.1. Actual solid contact proportion

Fig. 1 shows that the contact position of the mechanical joints is the tiny convex peak contact, and the contact gap is filled with lubricating oil. The oil medium steel-BMC mechanical joints consist of the steel-lubricating oil-BMC mechanical joints and the steel BMC mechanical joints. As shown in the figure, the deformation at the highest position of the tiny convex body is the largest under the pressure load, and the other deformation gradually decreases. As shown in the enlarged view, the larger the deformation, the darker the color.

The actual contact area of the mechanical joints is the foundation for analysing the mechanical joints performance [15–16]. To calculate the actual contact area of the mechanical joints, the maximum contact area of the tiny convex peak of the mechanical joints must be determined. However, it is difficult to find the maximum contact area of the tiny convex peak, which makes the accurate calculation very complex and difficult [17–18]. This paper will study the new calculation method.

For convenience of analysis, it is assumed that the contact imprint image of the mechanical joint is shown in **Fig. 2(a)**. The white area in the figure is the non-contact area, and the gray and black areas are the contact areas. The larger the contact deformation of the tiny convex peak in the contact area, the denser the contact degree, and the darker the contact color, even the blacker. On

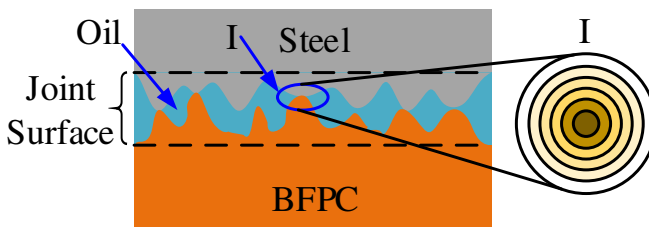
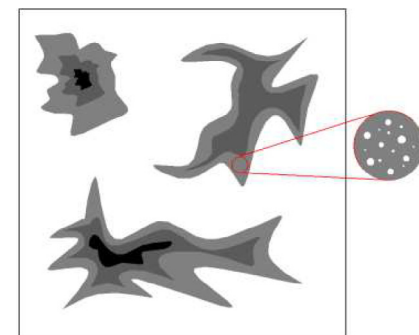
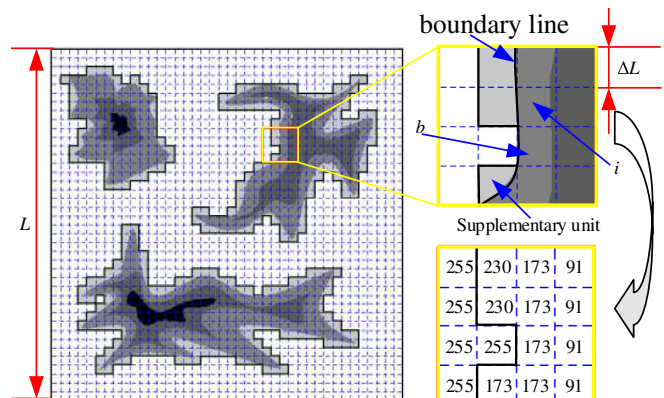


Fig. 1. Rough surface of mechanical joints.



(a) Contact imprint image



(b) Discrete division of contact imprints

Fig. 2. Discrete contact area division considering contact weights.

the contrary, the lighter the color, the less sufficient the contact, and even there will be non-contact holes in the contact area.

The contact imprinting image in **Fig. 2 (b)**, whose side length is L , is divided into n equal parts, and the image has n^2 discrete elements of square with side length $\Delta L = L/n$. Discrete elements are defined as contact elements or non-contact elements depending on whether they contain a contact area or not. According to the position of contact elements, they are divided into inner contact elements and boundary contact elements. The area enclosed by the yellow lines in the **Fig. 2 (b)** contains the inner contact element i (the surrounding elements are all contact elements) and the boundary contact element b (the surrounding elements have non-contact elements). After counting the amount of internal contact elements and boundary contact elements and multiplying by the element area, the contact area of the mechanical joints can be roughly calculated. The actual contact area of the boundary contact element is less than or equal to the area of the discrete element, as shown in the fourth row and second column of the yellow enlargement in **Fig. 2(b)**. The boundary line divides the element into contact and non-contact parts. According to the above rough calculation, the contact area obtained is the area of the gray area in the enlarged figure of **Fig. 2 (b)**, which leads to excessive calculation area.

The contact imprint image after grayscale processing is stored in MATLAB as grayscale value matrix, set as $H_{n \times n}$. As shown in the gray value matrix in **Fig. 2 (b)**, the gray value 255 represents the white area (non-contacted area), the gray value 0 represents the black area (contacted area, and the maximum contact density), and the other values are gray (contacted area, but the contact density is relatively small). To facilitate the analysis, the gray value

matrix is inversely processed. The value 255 is subtracted from the gray value matrix to obtain $\mathbf{C}_{n \times n}$

$$\mathbf{C}_{n \times n} = 255 - \mathbf{H}_{n \times n} \quad (1)$$

The gray value of elements in the non-contact region of matrix $\mathbf{C}_{n \times n}$ is zero. The gray value of the matrix $\mathbf{C}_{n \times n}$ contact region is non-zero, and the larger the gray value, the larger the contact deformation.

The inverse-treated contact imprint matrix $\mathbf{C}_{n \times n}$ is decomposed into internal contact element matrix and boundary contact element matrix.

$$\mathbf{C}_{n \times n} = \mathbf{I}_{n \times n} + \mathbf{B}_{n \times n} \quad (2)$$

where, $\mathbf{I}_{n \times n}$ is the internal contact element matrix, and $\mathbf{B}_{n \times n}$ is the boundary contact element matrix. After inversely processing, the gray value matrix of the region surrounded by yellow lines in Fig. 2 (b) is decomposed into the inner contact element matrix

$$\begin{bmatrix} 0 & 0 & 82 & 164 \\ 0 & 0 & 82 & 164 \\ 0 & 0 & 0 & 164 \\ 0 & 0 & 82 & 164 \\ \end{bmatrix} \text{ and boundary contact element matrix} \\ \begin{bmatrix} 0 & 25 & 0 & 0 \\ 0 & 25 & 0 & 0 \\ 0 & 0 & 82 & 0 \\ 0 & 82 & 0 & 0 \\ \end{bmatrix}.$$

There are numerous tiny pores in the contact element. To improve the accuracy of the calculation of the actual contact area, the affect of the contact weight of the contact elements should be taken into account. Divide the internal contact element matrix $\mathbf{I}_{n \times n}$ and boundary contact element matrix $\mathbf{B}_{n \times n}$ by the largest element in matrix $\mathbf{C}_{n \times n}$, and then sum the numerical values of all elements. The solid contact area of the mechanical joints considering the contact weight is obtained by discrete calculation method as

$$A_{rc} = \Delta L^2 \times \left(\sum_{s=1}^n \sum_{t=1}^n \frac{\mathbf{I}_{n \times n}}{\max(\mathbf{C}_{n \times n})} + \sum_{s=1}^n \sum_{t=1}^n \frac{\mathbf{B}_{n \times n}}{\max(\mathbf{C}_{n \times n})} \right) \quad (3)$$

The area of the discrete element is larger than the actual contact area of the boundary contact element, so Eq. (3) is improved

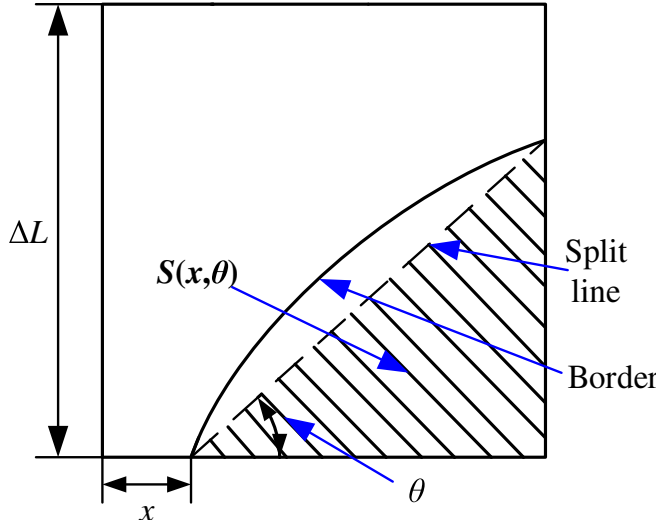


Fig. 3. Boundary contact element.

$$A_{rc} = \left(\sum_{s=1}^n \sum_{t=1}^n \frac{\mathbf{I}_{n \times n}}{\max(\mathbf{C}_{n \times n})} + \beta \sum_{s=1}^n \sum_{t=1}^n \frac{\mathbf{B}_{n \times n}}{\max(\mathbf{C}_{n \times n})} \right) \times \Delta L^2 \quad (4)$$

where, β is the contact proportion coefficient of boundary contact element.

As shown in Fig. 3, there are two intersections between the boundary line of the boundary contact element and the edge of the element. Connect the two intersections with a straight line to get a split line. The area enclosed by the split line and the discrete element boundary is $S(x, \theta)$. x and θ are uniformly distributed variables, so the area $S(x, \theta)$ is

$$S(x, \theta) = \begin{cases} \frac{1}{2}(\Delta L - x)^2 \tan \theta, & 0 < \theta \leq \arctan\left(\frac{\Delta L}{\Delta L - x}\right); \\ \Delta L^2 - x\Delta L - \frac{\Delta L^2}{2\tan\theta}, & \arctan\left(\frac{\Delta L}{\Delta L - x}\right) < \theta \leq \arctan\left(\frac{\Delta L}{x}\right), x < \frac{\Delta L}{2}; \\ x\Delta L + \frac{\Delta L^2}{2\tan\theta}, & \arctan\left(\frac{\Delta L}{\Delta L - x}\right) < \theta \leq \pi - \arctan\left(\frac{\Delta L}{x}\right), x < \frac{\Delta L}{2}; \\ \Delta L^2 - x\Delta L - \frac{\Delta L^2}{2\tan\theta}, & \arctan\left(\frac{\Delta L}{\Delta L - x}\right) < \theta \leq \pi - \arctan\left(\frac{\Delta L}{2x - \Delta L}\right), x \geq \frac{\Delta L}{2}; \\ x\Delta L + \frac{\Delta L^2}{2\tan\theta}, & \pi - \arctan\left(\frac{\Delta L}{2x - \Delta L}\right) < \theta \leq \pi - \arctan\left(\frac{\Delta L}{x}\right), x \geq \frac{\Delta L}{2}; \\ -\frac{1}{2}x^2 \tan \theta, & \pi - \arctan\left(\frac{\Delta L}{x}\right) < \theta < \pi \end{cases} \quad (5)$$

The average contact area of boundary contact element is

$$\bar{S} = \frac{1}{\pi \Delta L} \int_0^\pi \int_0^{\Delta L} S(x, \theta) dx d\theta \quad (6)$$

β is the ratio of \bar{S} to ΔL^2 . According to literature [19–20], it can be deduced that the β is

$$\beta = \frac{\bar{S}}{\Delta L^2} \approx 0.150387 \quad (7)$$

Because the split line is a straight line, and the boundary line is usually a curve, replace the triangle area with a quarter of the circular area as shown in Fig. 4, and the proportional relationship between them is

$$S' = \pi S_{\Delta}/2 \quad (8)$$

According to Eqs. (4), (7) and (8), the solid discrete contact area is

$$A_{rc} = \left(\sum_{s=1}^n \sum_{t=1}^n \frac{\mathbf{I}_{n \times n}}{\max(\mathbf{C}_{n \times n})} + \frac{\pi \beta}{2} \sum_{s=1}^n \sum_{t=1}^n \frac{\mathbf{B}_{n \times n}}{\max(\mathbf{C}_{n \times n})} \right) \times \Delta L^2 \quad (9)$$

The solid discrete contact proportion is

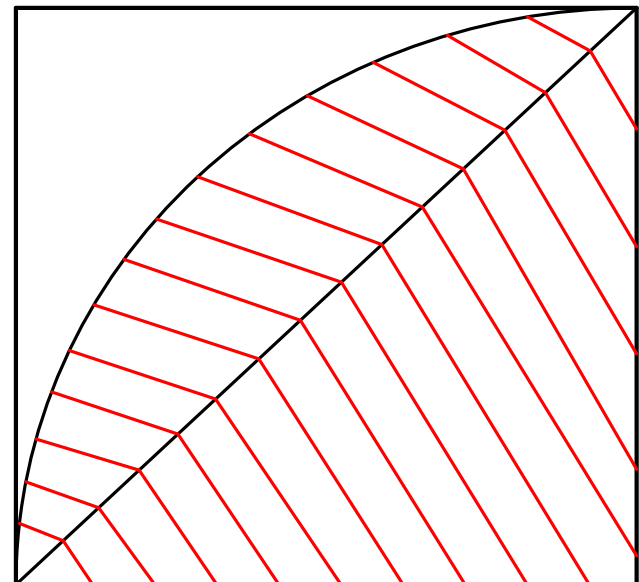


Fig. 4. Correction of boundary contact area.

$$R_{rc} = \frac{A_{rc}}{L^2}$$

$$= \left(\sum_{s=1}^n \sum_{t=1}^n \frac{\mathbf{I}_{n \times n}}{\max(\mathbf{C}_{n \times n})} + \frac{\pi\beta}{2} \sum_{s=1}^n \sum_{t=1}^n \frac{\mathbf{B}_{n \times n}}{\max(\mathbf{C}_{n \times n})} \right)$$

$$\times \left(\frac{\Delta L}{L} \right)^2 \quad (10)$$

The analysis shows that the equal parts n tends to infinity, the discrete element area tends to zero, and discrete contact proportion tends to the actual contact proportion.

2.2. Actual lubricating oil contact proportion

Lubricating oil is a liquid, and it has uniform contact with steel and BMC surfaces, so the actual contact area doesn't need to consider the influence of contact weight of lubricating oil. Due to the viscosity of lubricating oil, it is difficult for lubricating oil to penetrate into the micropores in the solid contact area of the steel-BMC mechanical joints. Therefore, when calculating the actual contact area of lubricating oil, its size is calculated by subtracting the actual solid contact area without considering the contact weight from the nominal contact area of the steel-BMC mechanical joints. The solid contact area without considering the contact weight is

$$A'_{rc} = \left(\text{Count}(\mathbf{I}_{n \times n}) + \frac{\pi\beta}{2} \text{Count}(\mathbf{B}_{n \times n}) \right) \times \Delta L^2 \quad (11)$$

where $\text{Count}(\mathbf{I}_{n \times n})$ and $\text{Count}(\mathbf{B}_{n \times n})$ are the number of non-zero elements of the internal contact element matrix $\mathbf{I}_{n \times n}$ and the boundary contact element matrix $\mathbf{B}_{n \times n}$, respectively.

The actual lubricating oil contact area is

$$A_{rl} = L^2 - A'_{rc} \quad (12)$$

The actual lubricating oil contact proportion is

$$R_{rl} = \frac{L^2 - A'_{rc}}{L^2}$$

$$= 1 - \left(\text{Count}(\mathbf{I}_{n \times n}) + \frac{\pi\beta}{2} \text{Count}(\mathbf{B}_{n \times n}) \right) \times \left(\frac{\Delta L}{L} \right)^2 \quad (13)$$

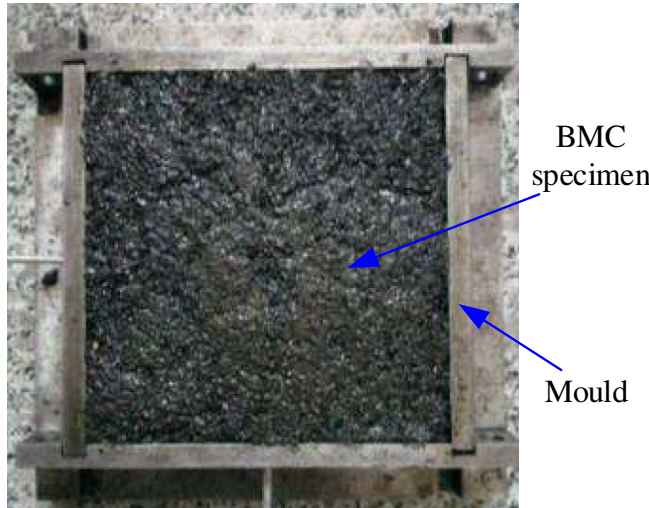


Fig. 5. BMC specimen and mould.

2.3. Analysis of actual contact proportion of solid and lubricating oil

The BMC specimens are manufactured by casting. The size of specimens is $150 \times 150 \times 20$ mm cubes. The specimen and mould are shown in Fig. 5. The BMC specimens are milled, and the roughness of machined specimens is $Ra3.2 \mu\text{m}$, $Ra6.3 \mu\text{m}$, $Ra12.5 \mu\text{m}$, respectively. The contact surface of the BMC specimens were evenly coated with red ink. The preload of $0.2 \text{ MPa} \sim 1 \text{ MPa}$ was applied to the steel-BMC mechanical joints using a hydraulic press to obtain the contact imprint images. The grayscale processed contact imprint images are shown in Fig. 6.

According to the process in Fig. 7, the actual solid contact proportion (with contact weight) and the actual lubricating oil contact proportion were calculated using MATLAB.

The roughness of steel specimens is $Ra3.2 \mu\text{m}$. The roughness of BMC specimens is $Ra6.3 \mu\text{m}$. Table 1 shows the discrete solid contact area under different conditions. Fig. 8 is the change curve of solid discrete contact proportion. The contact proportion function is obtained by MATLAB fitting, and its parameters are shown in Table 2.

$$R_{rcP} = \frac{p_1 n + p_2}{n + q} \quad (14)$$

where, p_1 , p_2 and q are fitting parameters, and P is preload of mechanical joints.

$n \rightarrow +\infty$, the actual solid contact proportion is

$$R_{cP} = \lim_{n \rightarrow +\infty} R_{rcP} = \lim_{n \rightarrow +\infty} \frac{p_1 n + p_2}{n + q} = p_1 \quad (15)$$

The roughness of steel specimens is $Ra3.2 \mu\text{m}$. The roughness of BMC specimens is $Ra6.3 \mu\text{m}$. The preloads of the steel BMC mechanical joints are $0.2 \text{ MPa} \sim 1 \text{ MPa}$, respectively. The actual solid contact proportion of steel BMC mechanical joints with contact weight are 2.03%, 2.877%, 3.628%, 4.468% and 4.859%, respectively. The actual solid contact proportion of steel BMC mechanical joints without contact weight is 3.56%, 4.497%,

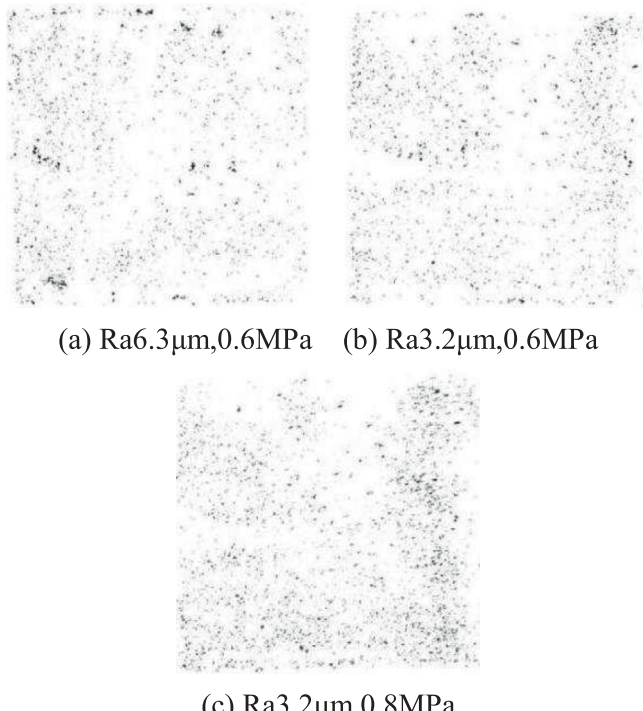


Fig. 6. Contact imprint image (grayscale processed).

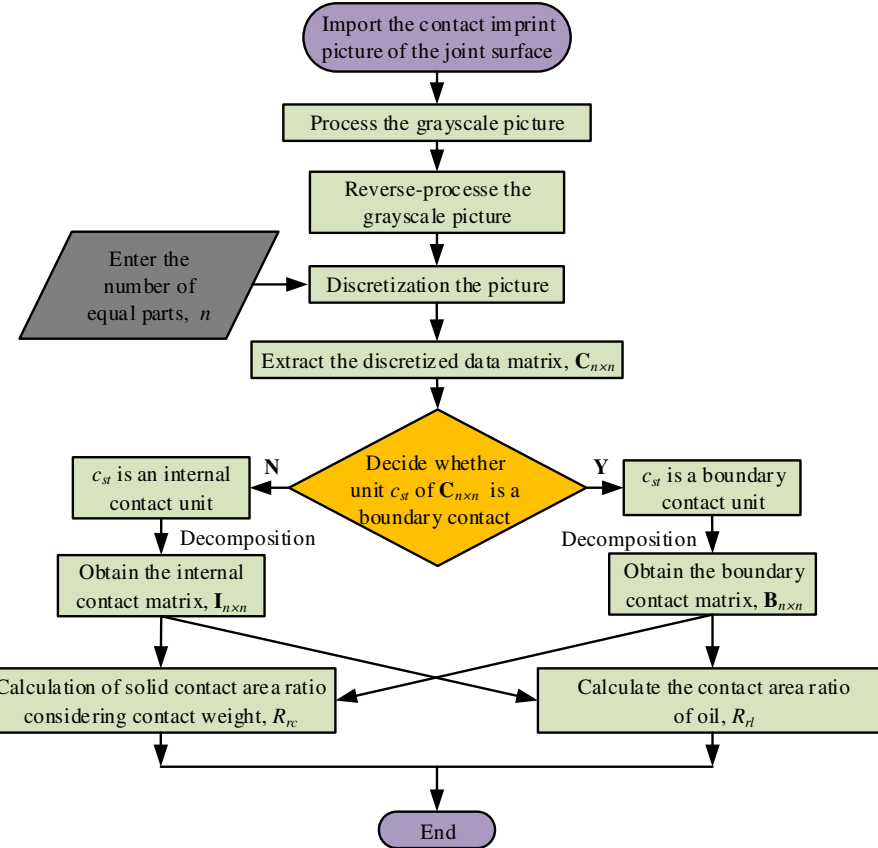
**Fig. 7.** Calculation Process.

Table 1
Discrete calculation results of solid contact proportion.

Preload/MPa	Equal fractions/n	With weight	Without weight	Preload/MPa	Equal fractions /n	With weight	Without weight
0.2	90	0.5134	0.5976	1.0	90	0.6625	0.8813
	120	0.4182	0.5180		120	0.5395	0.7718
	180	0.2662	0.3902		180	0.3722	0.5837
	240	0.2036	0.2939		240	0.2725	0.4534
	360	0.1482	0.2117		360	0.2109	0.3294
	720	0.0904	0.1484		720	0.1354	0.2308
	90	0.5612	0.7507		90	0.6995	0.9201
0.4	120	0.4613	0.6589		120	0.5767	0.8162
	180	0.2966	0.5015		180	0.4071	0.6191
	240	0.2264	0.3845		240	0.3052	0.4853
	360	0.1673	0.2762		360	0.2306	0.3513
	720	0.1061	0.1938		720	0.1505	0.2492
0.6	90	0.6211	0.8121	0.6	240	0.2518	0.4155
	120	0.5012	0.7055		360	0.1892	0.3012
	180	0.3295	0.5382		720	0.1168	0.2081

5.248%, 6.254% and 6.677%, respectively. Fig. 9 shows the curve of actual solid contact proportion and preload of BMC mechanical joints.

The actual solid contact proportion and the actual lubricating oil contact proportion of the steel BMC mechanical joints under different roughness and preload are obtained by the same calculation method. The results are shown in Table 3.

Fig. 10 shows the coupling effect of preload and roughness on the actual contact proportion of the mechanical joints. The figure shows that the actual solid contact proportion of the mechanical joints increases with the increase of preload, and reduces with increasing roughness. It can be seen from the figure that the influ-

ence of preload is greater than that of roughness. The actual contact proportion of lubricating oil is negatively related to the preload and positively related to the roughness value. The influence of preload is greater than roughness.

3. Theoretical model of thermal properties of mechanical joints

3.1. Equivalent thermal conductivity

As shown in Fig. 11, the heat conduction forms of the oil medium steel-BMC mechanical joints mainly include steel BMC heat conduction and steel-oil-BMC heat conduction. According to Four-

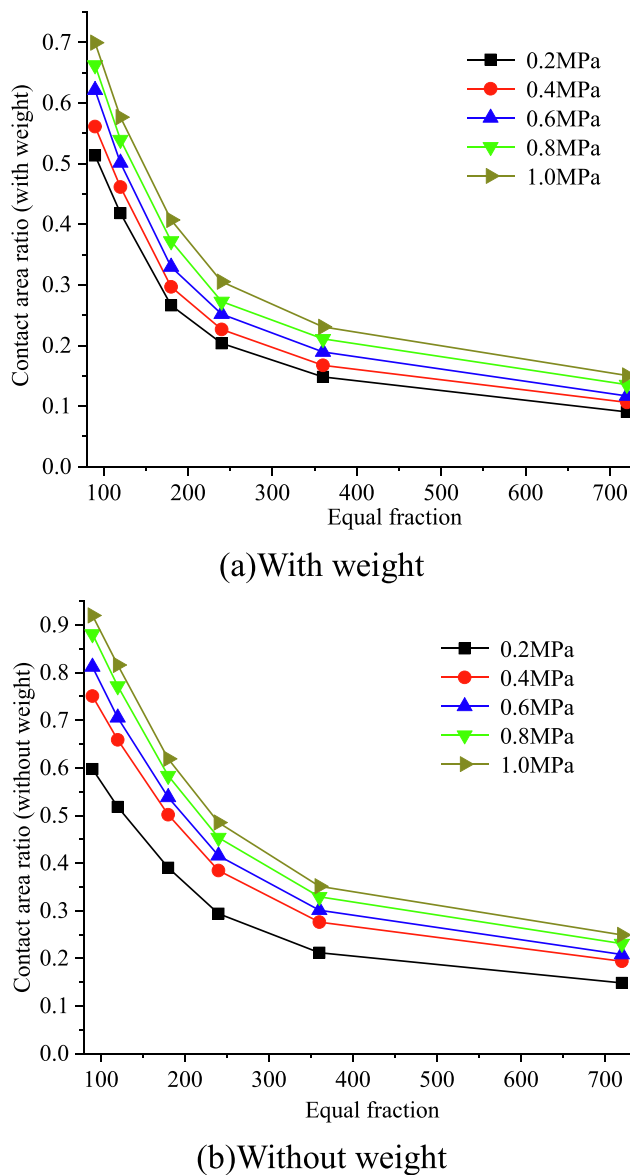


Fig. 8. Curve of discrete contact proportion.

ier heat conduction law, the relationship between heat flow and temperature difference and heat transfer area is as follows

$$\phi = -\lambda S dT/dx \quad (16)$$

where: ϕ is heat flow; λ is thermal conductivity; dT is temperature difference; dx is thickness of specimen; S is area of heat transfer.

The total heat flow of the oil medium steel-BMC mechanical joints is kept conservation [21]. According to energy balance for-

mula, the equivalent thermal conductivity of the oil medium steel-BMC mechanical joints is

$$\lambda_c = \frac{A_{rc}}{A} \frac{2\lambda_s \lambda_B}{\lambda_s + \lambda_B} + \frac{A_{rl}}{A} \lambda_o = R_{rc} \frac{2\lambda_s \lambda_B}{\lambda_s + \lambda_B} + R_{rl} \lambda_o \quad (17)$$

where, A is the nominal contact area of oil medium steel-BMC mechanical joints, L^2 ; λ_s , λ_B , λ_o are thermal conductivity of steel, BMC and oil, respectively.

3.2. Equivalent density

In Fig. 11, the equivalent thickness of steel specimen and BMC specimen is h_s and h_B , respectively. The sum of the lubricating oil mass m_o , the steel mass m_s , and the BMC mass m_B is divided by the equivalent volume V of the mechanical joints to obtain the equivalent density.

$$\rho_c = \frac{m_s + m_B + m_o}{V} = \frac{\rho_s A_{rc} h_s + \rho_B A_{rc} h_B + \rho_o A_{rl} (h_s + h_B)}{A(h_s + h_B)} = \frac{\rho_s R_{rc} h_s + \rho_B R_{rc} h_B + \rho_o R_{rl} (h_s + h_B)}{(h_s + h_B)} \quad (18)$$

where, ρ_s , ρ_B , ρ_o are the density of steel, BMC and lubricating oil.

3.3. Equivalent specific heat capacity

Because the thickness of the mechanical joints is very small, assume that the temperature changes of all components of the mechanical joints are equal to ΔT . The heat absorbed by the steel component of the oil medium steel-BMC mechanical joints is Q_s , the heat absorbed by the BMC component is Q_B , and the heat absorbed by the lubricating oil is Q_o . The equivalent specific heat capacity c_c of the oil medium steel-BMC mechanical joints is

$$c_c = \frac{Q_s + Q_B + Q_o}{m_c \Delta T} = \frac{c_s m_s \Delta T + c_B m_B \Delta T + c_o m_o \Delta T}{m_c \Delta T} = \frac{c_s \rho_s R_{rc} h_s + c_B \rho_B R_{rc} h_B + c_o \rho_o R_{rl} (h_s + h_B)}{\rho_c (h_s + h_B)} \quad (19)$$

where, c_s , c_B , c_o are the specific heat capacities of steel, BMC and lubricating oil.

3.4. Equivalent thickness

The equivalent thickness of steel and BMC is closely related to their surface roughness and tiny structure. The roughness of processed steel is $Ra3.2 \mu\text{m}$, and its equivalent thickness h_s is about 0.5 mm [22,23]. According to literature [22,23], it can be seen that surface roughness has a critical impact on equivalent thickness, and the relationship between them is proportional. The surface roughness of processed BMC specimens is about 1, 2, and 3 times that of steel specimens, so h_B of BMC is nearly 1, 2, and 3 times that of h_s respectively. The equivalent thickness of BMC is approximately 0.5 mm, 1 mm and 1.5 mm. The equivalent thickness of the mechanical joints is $h_c = h_s + h_B$.

Table 2
Fitting coefficient.

Preload/MPa	With weight			Without weight		
	$p_1/\times 10^{-2}$	p_2	q	$p_1/\times 10^{-2}$	p_2	q
0.2	2.030	46.64	2.995	3.56	79.05	45.47
0.4	2.877	50.92	3.837	4.497	106.7	55.12
0.6	3.628	54.88	2.56	5.248	112.9	52.93
0.8	4.468	61.31	7.488	6.254	121.5	52.06
1	4.859	70.25	15.55	6.677	132.8	58.16

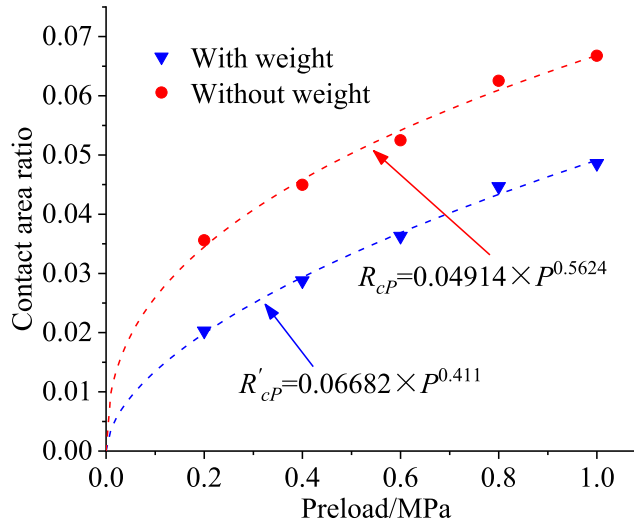


Fig. 9. Relationship between actual contact proportion and preload.

Table 3
Actual contact proportion of mechanical joints.

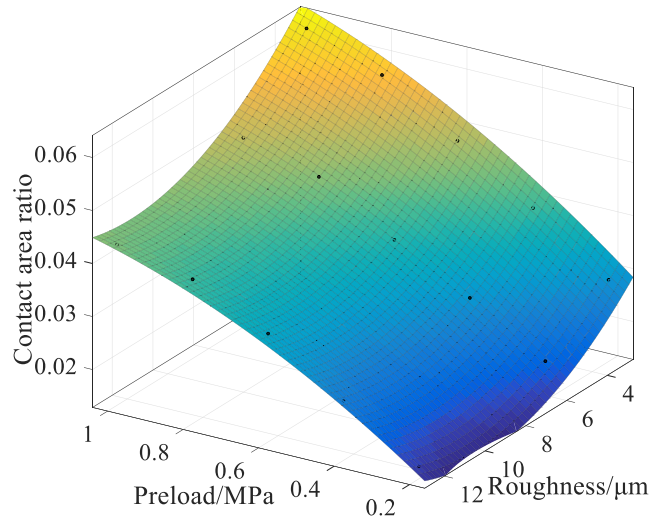
Preload/MPa	Roughness Ra/ μm	Solid	Lubricating oil
0.2	3.2	2.827%	95.756%
0.2	6.3	2.030%	96.44%
0.2	12.5	1.519%	97.02%
0.4	3.2	3.837%	94.772%
0.4	6.3	2.877%	95.503%
0.4	12.5	2.401%	96.162%
0.6	3.2	4.758%	93.618%
0.6	6.3	3.628%	94.752%
0.6	12.5	3.330%	95.317%
0.8	3.2	5.653%	92.679%
0.8	6.3	4.468%	93.746%
0.8	12.5	4.008%	94.501%
1.0	3.2	6.185%	92.141%
1.0	6.3	4.859%	93.323%
1.0	12.5	4.319%	94.118%

3.5. Variation law of equivalent thermal performance of mechanical joints

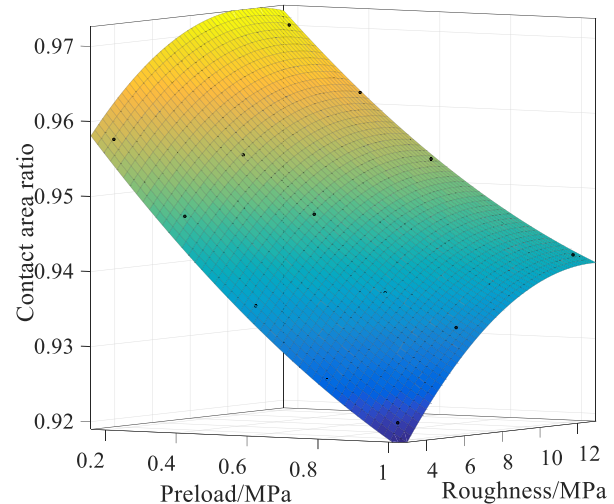
Table 4 shows the thermal performance parameters of steel, BMC and lubricating oil. According to Eqs. (17)~(19), the equivalent thermal performance parameters of the oil medium steel-BMC mechanical joints with different roughness and preload are calculated, as shown in Table 5.

Fig. 12 shows the equivalent thermal performance curve of the oil medium steel-BMC mechanical joints. According to Fig. 12(a)~(b), the equivalent thermal conductivity and equivalent density of the mechanical joints show rapid increase with increasing preload, but the increase rate gradually decreases. Equivalent thermal conductivity and equivalent density are inversely related to roughness. According to Fig. 12(c), the equivalent specific heat capacity decreases nonlinearly with the increase of preload. However, the specific heat capacity is the opposite.

Analyze the cause of thermal performance changes of oil medium steel-BMC mechanical joints. The actual solid contact proportion of the mechanical joints grows as the roughness falls or as the preload grows. The thermal properties of mechanical joints tend to be the properties of solid material (BMC and steel) with the increase of the actual solid contact proportion. The thermal conductivity and density of solid materials (steel and BMC) is much greater than that of lubricants oil, so the relevant performance



(a) Solid contact proportion



(b) Lubricating oil contact proportion

Fig. 10. Coupling effect of preload and roughness.

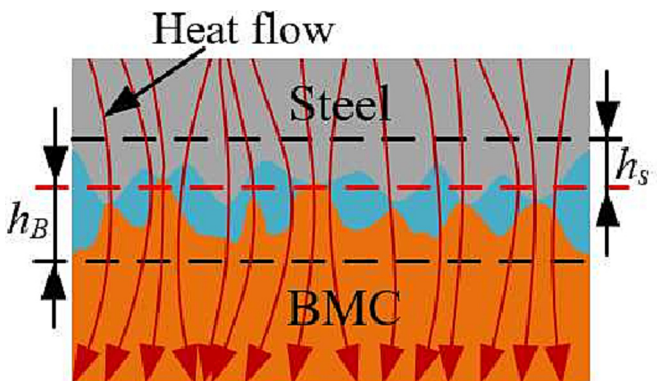


Fig. 11. Heat conduction forms of mechanical joints.

parameters of mechanical joints increase with the proportion of solids in contact. However, the equivalent specific heat capacity of the oil medium steel-BMC mechanical joints is the reverse.

Table 4
Material parameters.

	Thermal conductivity/W·(m·K) ⁻¹	Specific heat capacity/kJ·(kg·K) ⁻¹	Density/kg·m ⁻³
Steel	45	0.46	7850
BMC	1.5134	1.07	2850
Oil	0.1324	1.87	873

Table 5
Performance parameters of mechanical joints.

Preload/MPa	Roughness/μm	Equivalent thermal conductivity/W·(m·K) ⁻¹	Equivalent density/kg·m ⁻³	Equivalent specific heat capacity/kJ·(kg·K) ⁻¹
0.2	3.2	0.20956	987.19438	1.67887
0.2	6.3	0.18713	933.60953	1.75673
0.2	12.5	0.17294	909.26360	1.79521
0.4	3.2	0.23784	1032.63906	1.62200
0.4	6.3	0.21069	963.68569	1.71447
0.4	12.5	0.19763	937.93526	1.75539
0.6	3.2	0.26328	1071.83814	1.57372
0.6	6.3	0.23169	991.04963	1.67929
0.6	12.5	0.22371	968.64741	1.71609
0.8	3.2	0.28824	1111.52317	1.53056
0.8	6.3	0.25496	1020.20725	1.64185
0.8	12.5	0.24249	989.32173	1.68862
1.0	3.2	0.30311	1135.28843	1.50639
1.0	6.3	0.26585	1034.17462	1.62524
1.0	12.5	0.25109	998.72914	1.67639

4. Virtual material simulation method of mechanical joints

In order to accurately simulate and analyse the thermal and thermomechanical coupling properties of oil medium steel-BMC mechanical joints. The application of virtual material simulation method to the analysis of oil medium steel-BMC mechanical joints was investigated. The oil medium steel-BMC mechanical joint was simulated with a layer of uniform virtual material [9,24], as shown in Fig. 13. Virtual materials' thermal performance parameters are described in Section 3. In addition, the theoretical models of equivalent elastic modulus, equivalent expansion coefficient and Poisson's ratio of virtual materials need to be derived.

4.1. Virtual materials' equivalent elastic modulus

The elastic modulus is the proportion of normal stress σ to normal strain ε . The normal stress is the proportion of the normal load F_n to the area A of force action. The normal strain ε is the proportion of the compression deformation $\Delta\delta_c$ to the equivalent thickness h_c of the mechanical joints. The compression deformation $\Delta\delta_c$ of the mechanical joints is negatively related to the equivalent stiffness K_n .

$$E_c = \frac{\sigma}{\varepsilon} = \frac{F_n/A}{\Delta\delta_c/h_c} = \frac{F_n h_c}{A \Delta\delta_c} = \frac{F_n h_c}{A} \times \frac{1}{F_n/K_n} = \frac{K_n h_c}{A} \quad (20)$$

The equivalent stiffness K_n of the oil medium steel-BMC mechanical joints is provided by the solid contact stiffness and the lubricating oil contact stiffness, and they are in parallel. K_n is

$$K_n = K_{s-B} + K_o \quad (21)$$

where, K_{s-B} is the contact stiffness provided by solid materials, and K_o is the contact stiffness provided by lubricating oil.

The solid contact stiffness of mechanical joints can be obtained from the fractal contact theory.

$$K_{s-B} = E\sqrt{A} \times K_{s-B}^* \\ = \frac{2E\sqrt{A}}{\sqrt{\pi}} \cdot g(D) \cdot R_{rc}^{\frac{D}{2}} \cdot \left[\left(\frac{2-D}{D} \right)^{\frac{1-D}{2}} \cdot R_{rc}^{\frac{1-D}{2}} - a_c^{*\frac{1-D}{2}} \right] \quad (22)$$

where, K_{s-B}^* is the dimensionless contact stiffness. $g(D)$ is the parameter, $g(D) = (2-D)^{\frac{D}{2}} \cdot D^{\frac{2-D}{2}} \cdot (D-1)^{-1}$. D is the fractal dimension of the BMC rough surface. E is the equivalent elastic modulus, $E^{-1} = (1-v_1^2)E_1^{-1} + (1-v_2^2)E_2^{-1}$. v_1 , v_2 , E_1 and E_2 are Poisson's ratio and elastic modulus of steel and BMC respectively. a_c^* is the dimensionless critical contact area, $a_c^* = G^{-2} \cdot [H/(2E)]^{-\frac{2}{D-1}}$. H is the hardness of BMC. G^* is the dimensionless characteristic scale parameter of BMC rough surface, $G^* = G/\sqrt{A_n}$. G is the characteristic scale parameter of BMC rough surface.

It is assumed that there is no leakage of lubricating oil on the mechanical joints. According to the bulk elastic modulus of lubricating oil, its elastic modulus is deduced as

$$E_o = V_o \frac{\Delta p_o}{\Delta V_o} = (A_{rl}h_c) \times \frac{\Delta F/A_{rl}}{\Delta A_{rl}\Delta\delta} = \frac{h_c K_o}{A_{rl}} \quad (23)$$

where, E_o is the elastic modulus of lubricating oil, 1.5GPa. V_o is the volume of lubricating oil in the mechanical joints. Δp_o is the change pressure on the lubricating oil. ΔV_o is the change volume of lubricating oil after pressure. ΔF is the normal support force provided by the lubricating oil. $\Delta\delta$ is the change of oil film thickness after the mechanical joints is compressed.

The contact stiffness provided by the lubricating oil is

$$K_o = A_{rl}E_o/h_c \quad (24)$$

In fact, the lubricating oil in the mechanical joints is not completely sealed, taking into account the influence of lubricant leakage, Eq. (24) is modified as

$$K_o = \gamma A_{rl}E_o/h_c \quad (25)$$

where, γ is the leakage coefficient, dependent on the roughness and geometry of the mechanical joints, 0.421[25].

According to Eqs. (20)~(22) and Eq. (25), the total normal stiffness of oil medium steel-BMC mechanical joints is

$$E_c = \frac{2Eh_c}{\sqrt{A}\pi} \cdot g(D) \cdot R_{rc}^{\frac{D}{2}} \cdot \left[\left(\frac{2-D}{D} \right)^{\frac{1-D}{2}} \cdot R_{rc}^{\frac{1-D}{2}} - a_c^{*\frac{1-D}{2}} \right] + \gamma R_{rl}E_o \quad (26)$$

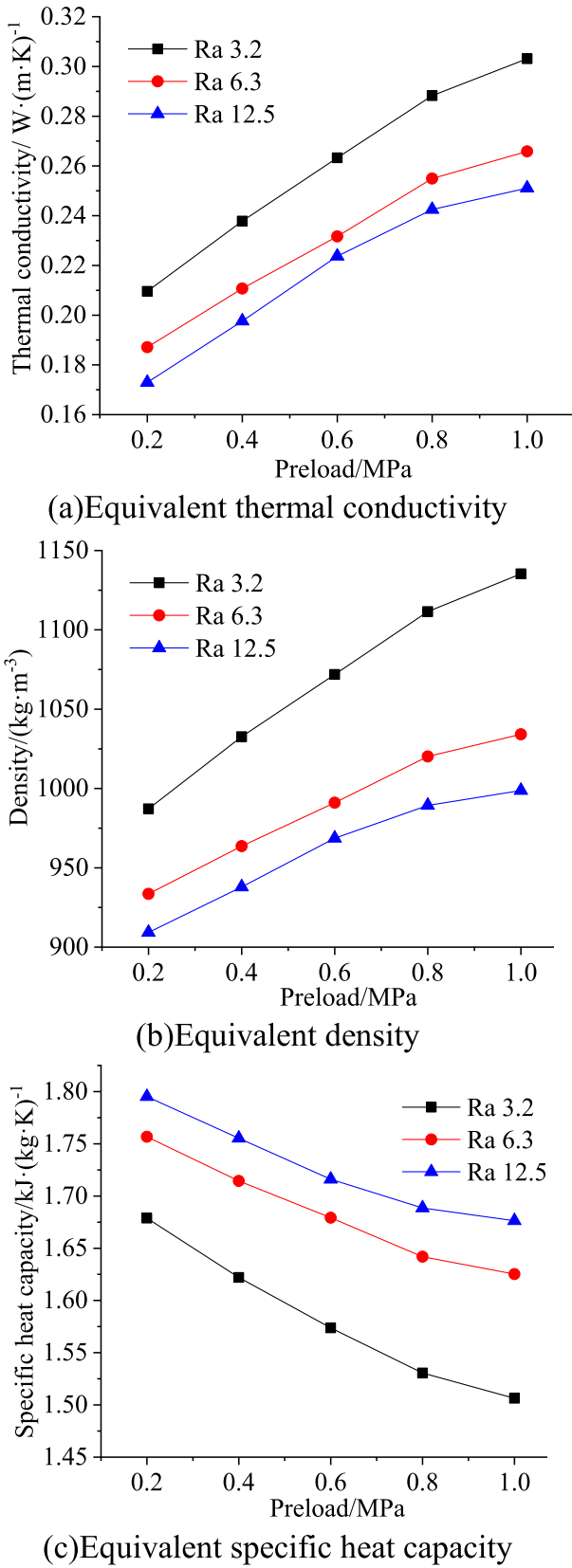


Fig. 12. Thermal performance parameters of mechanical joints.

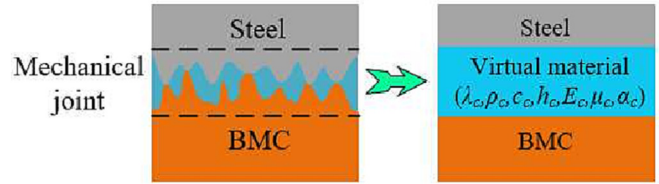


Fig. 13. Virtual material model of mechanical joints.

4.2. Virtual materials' equivalent expansion coefficient

The oil medium steel-BMC mechanical joints are composed of lubricating oil, steel and BMC. The equivalent expansion coefficient of oil medium steel-BMC mechanical joints is equal to the algebraic sum of the product of the volume fraction of each component and its expansion coefficient [26].

$$\alpha_c = \frac{A_{Rl}h_s}{Ah_c}\alpha_s + \frac{A_{Rl}h_B}{Ah_c}\alpha_B + \frac{\gamma A_{Rl}h_c}{Ah_c}\alpha_o \\ = \frac{R_{Rl}h_s}{h_c}\alpha_s + \frac{R_{Rl}h_B}{h_c}\alpha_B + \gamma R_{Rl}\alpha_o \quad (27)$$

Where, α_s is the expansion coefficient of steel, α_B is the expansion coefficient of BMC, and α_o is the expansion coefficient of lubricating oil.

4.3. Virtual materials' equivalent Poisson's ratio

The Poisson's ratio is the ratio of tangential deformation to the normal deformation. As the contact of the mechanical joints is incomplete, the transverse deformation of the tiny convex peak by the force will fill the gap of tiny convex peaks. On the whole, there is essentially no deformation in the tangential direction of the mechanical joints. The equivalent Poisson's ratio μ_c is zero.

4.4. Theoretical verification of thermal performance of mechanical joints

4.4.1. Simulation study

To test the accuracy of the above study, the temperature variation of the oil medium steel-BMC mechanical joints which heated with 39.84 W for 600 s was studied by simulation and experiment respectively.

The BMC specimen is a cuboid with a size of 150 × 150 × 20 mm, its roughness is Ra6.3 μm, and its fractal parameters are D = 1.17 and G = 2.8. The hardness of BMC material is 45 MPa, its elastic modulus is 35GPa, its Poisson's ratio is 0.26, and its expansion coefficient is $2.48 \times 10^{-6}/K$. The steel specimen is a cuboid with a size of 150 × 150 × 10 mm. The roughness of steel specimen is Ra3.2 μm. Its elastic modulus is 200GPa, its Poisson's ratio is 0.27, and its expansion coefficient is $1.17 \times 10^{-5}/K$.

Table 6
Equivalent parameters of the virtual material.

Thermal conductivity/ W·(m·K) ⁻¹	Specific heat capacity/ kJ·(kg·K) ⁻¹	Density/ kg·m ⁻³	Thickness/ mm
0.255	1.6419	1020.2173	1.5
Elastic modulus/MPa	Expansion coefficient/K	Poisson's ratio	—
828.51	2.53×10^{-4}	0	—

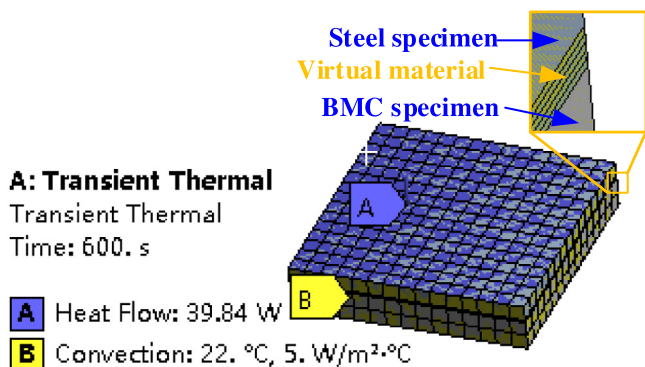


Fig. 14. Simulation analysis model.

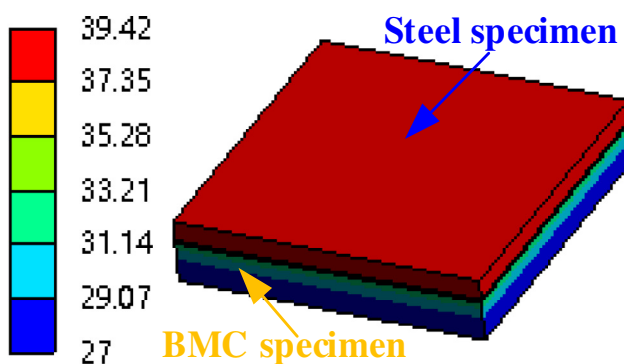


Fig. 15. Temperature analysis results.

The bulk modulus of elasticity of lubricating oil is 1.5GPa, and its expansion coefficient is $6.4 \times 10^{-4}/\text{K}$.

The preload of the oil medium steel-BMC mechanical joints was 0.8 MPa. The solid contact proportion is 0.04468, and the actual lubricating oil contact proportion is 0.93746. The equivalent parameters of the virtual material are shown in Table 6.

Creo software was used to draw the 3D model of virtual material specimen. In the software, a 1.5 mm thin layer was cut on the mechanical joints as a virtual material layer which uses boolean operations. The 3D model was imported into Workbench software

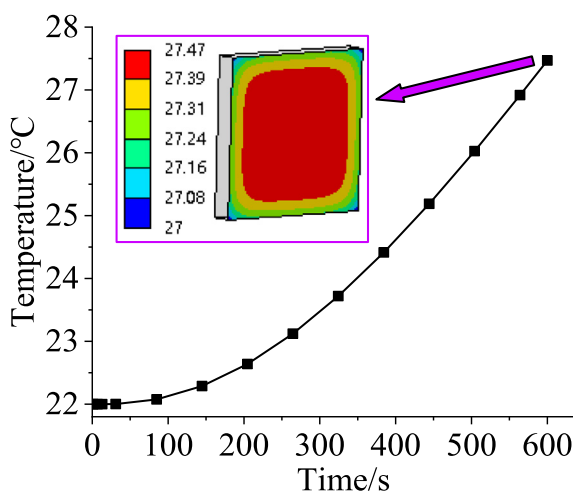


Fig. 16. Highest temperature on the bottom of BMC specimen.

and assigned material properties according to Table 6. The upper surface of the steel specimen was subjected to a thermal power of 39.84 W. Because of the air heat dissipation, the heat dissipation power of $5 \text{ W}/(\text{m}^2 \cdot \text{°C})$ is received around the mechanical joint specimen. Fig. 14 shows the setup of the simulation analysis model. Fig. 15 shows the overall temperature of the mechanical joint specimen.

The result of the analysis shows that the highest temperature of the model was 39.42°C, located on the upper surface of the steel specimen, and the lowest temperature of the model was 27°C, located on the bottom surface of the BMC specimen. The highest temperature change of BMC specimen within 600 s is shown in the curve in Fig. 16. Because there was air cooling around the specimen, the highest temperature at the center of the bottom surface of BMC was 27.47 °C.

4.4.2. Experimental verification

As shown in Fig. 17 (The figure is the middle section of the experimental facility), a resistance heating film was placed at the bottom of the oil medium steel-BMC specimen. In order to prevent the heat loss of the heating film, adiabatic asbestos was used to insulate the bottom of the heating film. To prevent heat transfer to the pressure plate, a adiabatic asbestos was used between the BMC specimen and the pressure plate. A thermocouple temperature sensor was used to check the temperature at the center of the contact surface between the BMC specimen and the adiabatic asbestos. The voltage through the heating film was 20.55 V. The resistance of the heating film was 10.6Ω and the power of the heating film was calculated to be 39.84 W based on the applied voltage. The experimental heating power was the same as that of the simulation. The temperature change of BMC specimen was detected within 600 s, and the BMC temperature was recorded every 30 s.

Fig. 18 is the experimental device. Fig. 19 is the temperature curve of the BMC specimen. The ambient temperature during both simulation and experiment is 22°C. The simulation results and experimental results almost coincided within 300 s, and then the temperature of the simulation results rose rapidly, but the change trend of experimental results and simulation results was consistent. The highest temperature of the contact surface between the BMC specimen and the adiabatic asbestos measured at 600 s was 26.9°C, and the relative error with the simulation was only -2.1% . The experimental temperature was slightly lower than the simulation temperature because the asbestos can't be completely insulated, and part of the heat loss caused the experimental temperature to be slightly lower. However, the experimental results can still prove the accuracy of the thermal performance simulation analysis method and a theoretical model of the oil medium steel-BMC mechanical joints.

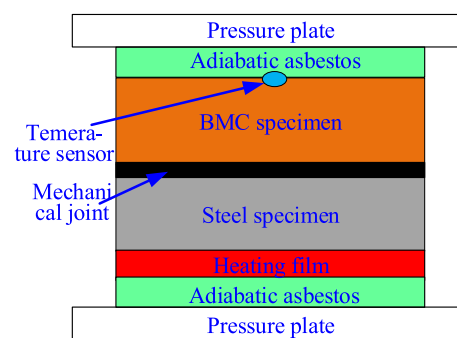


Fig. 17. Basic principle of experiment.

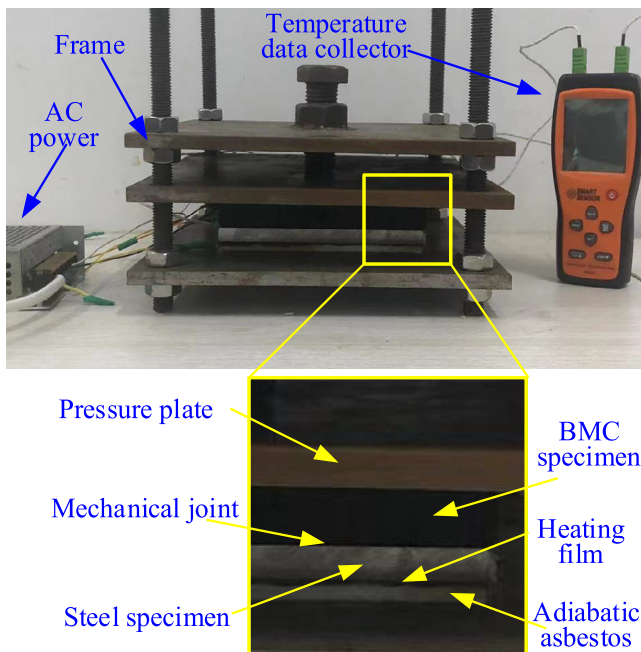


Fig. 18. Experimental detection device.

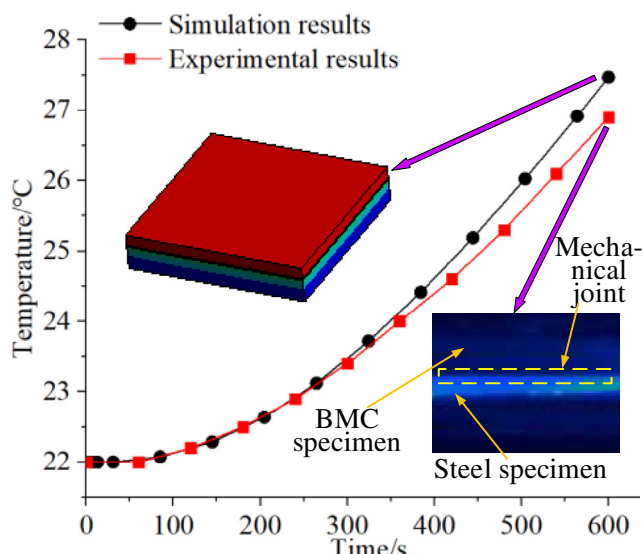


Fig. 19. Result comparison.

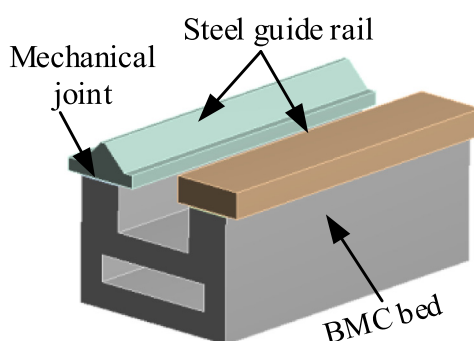


Fig. 20. BMC bed foundation.

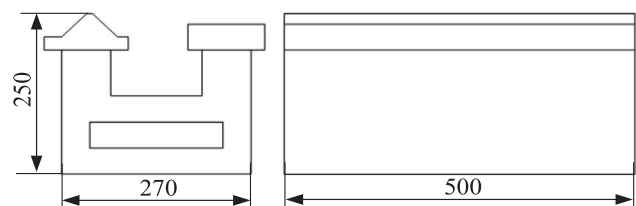


Fig. 21. Dimensions of the BMC bed foundation.

The temperature distribution of the oil medium steel-BMC mechanical joint specimens was examined by the infrared thermography. The results are shown in Fig. 19. According to the infrared image, the temperature at the junction of steel and BMC specimen dropped sharply, and the infrared temperature distribution was consistent with the simulation temperature distribution.

5. Example analysis

Fig. 20 shows the BMC bed foundation, the BMC bed foundation consists of the BMC bed and steel guide rails. The dimensions of the BMC bed foundation are shown in Fig. 21. The steel guide rail contacts the BMC bed to form an oil medium steel-BMC mechanical joints. According to the cutting force and self weight of the machine tool, the friction coefficient of the guide rail, and the maximum feed speed, the maximum heating power of the machine tool guide rail is calculated to be about 400 W. The performance parameters of oil medium steel-BMC mechanical joints are the same as those in Section 4.4.1. The thermal performance and thermal mechanical coupling performance of the BMC bed base foundation with and without the mechanical joints in 0 ~ 1200 s were studied by simulation.

When considering the influence of oil-mediated steel-BMC mechanical joints, a 1.5 mm thick virtual material layer was cut at the contact position of the mechanical joints. The material parameters for each part of the BMC bed foundation and the virtual material layer were defined during simulation analysis. The mesh size is 10 mm, and automatic division is used for mesh division. The model contains 103,149 nodes and 20,825 elements. A thermal power load of 400 W is applied to the surface of the rails. The BMC bed is subjected to 5 W/(m²·°C) of heat dissipation power. The fixed constraint was applied on the bottom of the BMC bed. The same method was used to define the material parameters, the constraints and boundary conditions respectively for the model ignoring the oil-mediated steel-BMC mechanical joints, and the constraints and boundary conditions are the same as when considering the oil-mediated steel-BMC mechanical joints. Fig. 22 shows the temperature results of the BMC bed foundation at 1200 s. The highest temperature of the model without considering the mechanical joints was 47.98°C. The highest temperature of the

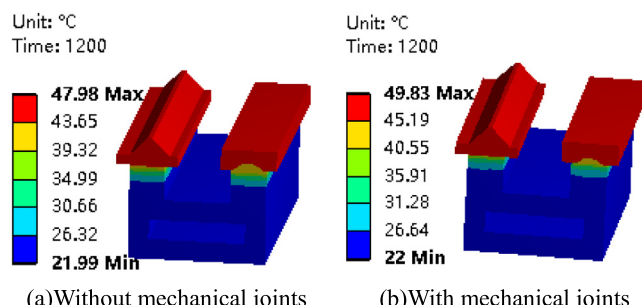


Fig. 22. Temperature results at 1200 s.

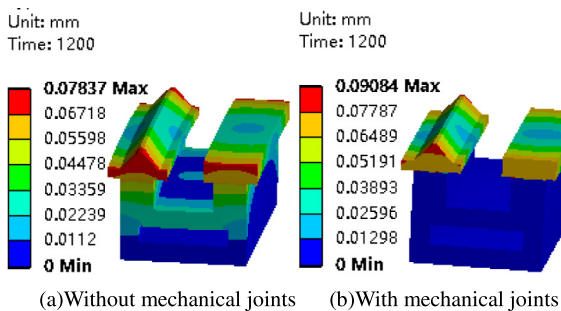


Fig. 23. Thermal deformation at 1200 s.

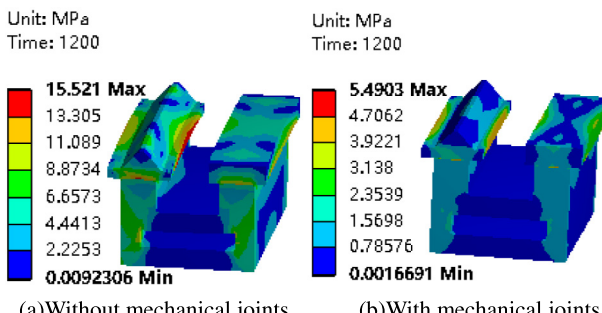


Fig. 24. Thermal stress at 1200 s.

model considering the mechanical joints was 49.83 °C. The relative change rate of the highest temperature is + 3.9%.

Fig. 23 shows the maximum thermal deformation of the BMC bed foundation affected by thermal mechanical coupling. Without considering the mechanical joints, maximum thermal deformation of the BMC bed foundation is 0.07837 mm. The maximum thermal deformation of the BMC bed foundation considering the mechanical joints is 0.09084 mm. The relative change rate of the maximum thermal deformation is + 15.9%. Fig. 24 shows the maximum thermal stress of the BMC bed foundation affected by thermal mechanical coupling. The maximum thermal stress of the BMC bed foundation without considering the mechanical joints is 15.521 MPa. The maximum thermal stress of the BMC bed foundation considering the mechanical joints is 5.4903 MPa. The relative change rate of the maximum thermal stress is -64.6%.

6. Conclusion

A discrete analytical method for the actual contact proportion of the oil medium steel-BMC mechanical joints considering the contact weight was established. The effects of the preload and roughness of the mechanical joints on the equivalent thermal performance of the oil medium steel-BMC mechanical joints was analyzed. A virtual material-simulation analysis method for oil medium steel-BMC mechanical joints considering contact weights has been developed. The accuracy of the study was verified through simulation and experiment. The conclusions are as follows:

(1) The actual solid contact proportion of the mechanical joints increases as the roughness decreases or the preload increases, and the effect of preload is greater than that of roughness. The actual lubricating oil contact proportion is negatively related to the preload, and positively related to the roughness, and the pressure load has a greater impact.

(2) The equivalent density and the equivalent thermal conductivity of the oil medium steel-BMC mechanical joints have similar

changing laws. They increase nonlinearly with the increase of the preload of the mechanical joints. They increase as the surface quality of the mechanical joints increases. The equivalent specific heat capacity of the mechanical joints decreases nonlinearly with the increase of preload. However, its performance decreases with increasing surface quality.

(3) The temperature rise of the oil medium steel-BMC mechanical joints specimen was studied by virtual material simulation analysis method and the experimental method respectively. The relative error of highest temperature of the two methods is only -2.1%, which prove the accuracy of this study.

(4) The thermal performance and thermal mechanical coupling performance of BMC bed foundation were studied with and without considering the influence of oil medium steel-BMC mechanical joints. The results showed that the highest temperature relative error is +3.9%, the maximum thermal deformation relative error is +15.9%, and the maximum thermal stress relative error is -64.6% with the same load and boundary conditions. It is proved that the oil medium steel-BMC mechanical joints have a key influence on the thermal performance and thermal mechanical coupling performance of the machine tool.

Declaration of Competing Interest

The authors declare that they have no known competing financial interests or personal relationships that could have appeared to influence the work reported in this paper.

Acknowledgments

The present work is supported by National Natural Science Foundation of China (52005238), Doctor Initiation Fund of Science and Technology Department of Liaoning Province (2020-BS-256).

References

- [1] H.-C. Möhring, C. Brecher, E. Abele, J. Fleischer, F. Bleicher, Materials in machine tool structures, *CIRP Ann.* 64 (2) (2015) 725–748.
- [2] D.I. Kim, S.C. Jung, J.E. Lee, S.H. Chang, Parametric study on design of composite-foam-resin concrete sandwich structures for precision machine tool structures, *Compos. Struct.* 75 (1-4) (2006) 408–414.
- [3] D. Kono, S. Mizuno, T. Muraki, M. Nakaminami, A machine tool motorized spindle with hybrid structure of steel and carbon fiber composite, *CIRP Ann.* 68 (1) (2019) 389–392.
- [4] P. Dunaj, T. Okulik, B. Powalka, et al. Experimental investigations of steel welded machine tool bodies filled with composite material, *International Scientific-Technical Conference MANUFACTURING*, Springer, Cham. 61-69 2019.
- [5] E.F. Kushnir, M.R. Patel, T.M. Sheehan, Material considerations in optimization of machine tool structure, *ASME International Mechanical Engineering Congress and Exposition*, Am. Soc. Mech. Eng. 35746 (2001) 133–145.
- [6] J. Yin, J. Zhang, W. Wang, X. Ren, Effect of glass fiber surface treatment on the mechanical strength of glass fiber reinforced resin mineral composite for machine tool bed, *Polym. Compos.* 38 (8) (2017) 1559–1570.
- [7] J. Shen, P. Xu, Y. Yu, Dynamic Characteristics Analysis and Finite Element Simulation of Steel-BFPC Machine Tool Mechanical joints, *J. Manuf. Sci. Eng.* 142 (1) (2020) 011006.
- [8] Y. Chang, J. Ding, Z. He, et al., Effect of joint interfacial contact stiffness on structural dynamics of ultra-precision machine tool, *Internat. J. Machine Tools Manuf.* 158 (2020).
- [9] H. Tian, B. Li, H. Liu, et al., A new method of virtual material hypothesis-based dynamic modeling on fixed mechanical joints in machine tools, *Int. J. Mach. Tool Manu.* 51 (3) (2011) 239–249.
- [10] Q. Chen, F. Xu, P. Liu, et al., Research on fractal model of normal contact stiffness between two spheroidal mechanical joints considering friction factor, *Tribology Internat.* 97 (2016) 253–326.
- [11] J. Liu, C. Ma, S. Wang, S. Wang, B.o. Yang, H.u. Shi, Thermal-structure interaction characteristics of a high-speed spindle-bearing system, *Int. J. Mach. Tool Manu.* 137 (2019) 42–57.
- [12] S.N. Shoukry, R.H. Thorneley, Theoretical expressions for the normal and tangential stiffness of machine tool joints, in: *Proceedings of the Twenty-second International Machine Tool Design and Research Conference*, Palgrave, London, 1982, pp. 131–138.

- [13] A. Archenti, M. Nicolescu, A top-down equivalent stiffness approach for prediction of deviation sources in machine tool joints, *CIRP Ann.* 66 (1) (2017) 487–490.
- [14] Y. Zhao, C. Yang, L. Cai, W. Shi, Z. Liu, Surface contact stress-based nonlinear virtual material method for dynamic analysis of bolted joint of machine tool, *Precis. Eng.* 43 (2016) 230–240.
- [15] R. Wang, L. Zhu, C. Zhu, Research on fractal model of normal contact stiffness for mechanical joint considering asperity interaction, *Int. J. Mech. Sci.* 134 (2017) 357–369.
- [16] X. Zhang, N. Wang, G. Lan, et al., Tangential damping and its dissipation factor models of mechanical joints based on fractal theory with simulations, *J. Tribol.* 136 (1) (2014) 011704.
- [17] S.Y. Jiang, Y.J. Zheng, H. Zhu, A contact stiffness model of machined plane joint based on fractal theory, *J. Tribol.-Trans. ASME* 132 (1) (2010) 1–7.
- [18] K. Konowalski, Experimental research and modeling of normal contact stiffness and contact damping of machined mechanical joints, *Adv. Manuf. Sci. Technol.* 33 (3) (2009) 53–68.
- [19] V.A. Yastrebov, G. Anciaux, J.F. Molinari, On the accurate computation of the true contact-area in mechanical contact of random rough surfaces, *Tribol. Int.* 114 (2017) 161–171.
- [20] J.X. Shen, Z.H. Pan, P. Xu, et al., Theoretical modelling and simulation analysis of the thermal performance of a steel-basalt fiber polymer concrete machine tool mechanical joints, *J. Mech. Sci. Technol.* 36 (7) (2022) 3753–3765.
- [21] W.L. Gu, Y.S. Yang, The influence of temperature on contact resistance of metallic surfaces temperature, *Trans. Nanjing Univ. Astronaut. Astronaut.* 26 (1994) 342–350.
- [22] H.L. Tian, F.R. Liu, Z.F. Fang, et al., Immovable mechanical joint's model using isotropic virtual material, *J. Vib. Eng.* 137 (2019) 42–57.
- [23] X.P. Li, H. Guo, J.N. Liu, et al., Fractal model and simulation of normal contact stiffness considering the friction between mechanical joints, *J. Vib. Measure. Diag.* 33 (2) (2013) 211–1123.
- [24] J.D. Suh, G.L. Do, Thermal characteristics of composite sandwich structures for machine tool moving body applications, *Compos. Struct.* 66 (1–4) (2004) 429–438.
- [25] Cameron, Basic lubrication theory, Ellis Horwood Press, London, 1981.
- [26] T.K. Dey, M. Tripathi, Thermal properties of silicon powder filled high-density polyethylene composites, *Thermochim. Acta* 502 (1–2) (2010) 35–42.